Scientific Research Publishing

Open Journal of Composite Materials, 2026, 16(2), 37-58
https://www.scirp.org/journal/ojcm
ISSN Online: 2164-5655
ISSN Print: 2164-5612

Microstructural and Thermal Characterization of *Hyphaene thebaica* Fibers from the Far North of Cameroon with a View to Their Incorporation into Polymer Matrices

Kabé Adama[1], Valentin Makomra[2], Memtine Ndong Augustin[1], Frédéric Djoda Pagore[3*], Omolola E. Fayemi[4,5], Hambaté Gomdjé Valery[1], Moussa Sali[3]

[1]Department of Textile and Leather Engineering, National Advanced School of Engineering, University of Maroua, Maroua, Cameroon
[2]Department of Civil Engineering, National Advanced School of Public Works, Yaoundé, Cameroon
[3]Department of Civil Engineering and Architecture, National Advanced School of Engineering, University of Maroua, Maroua, Cameroon
[4]Department of Chemistry, School of Physical and Chemical Sciences, Faculty of Natural and Agricultural Sciences, North-West University (Mafikeng Campus), Mmabatho, South Africa
[5]Material Science Innovation and Modelling (MaSIM) Research Focus Area, Faculty of Natural and Agricultural Sciences, North-West University (Mafikeng Campus), Mmabatho, South Africa
Email: *frederic.djodap@univ-maroua.cm, djodap@yahoo.fr

How to cite this paper: Adama, K., Makomra, V., Augustin, M.N., Pagore, F.D., Fayemi, O.E., Valery, H.G. and Sali, M. (2026) Microstructural and Thermal Characterization of *Hyphaene thebaica* Fibers from the Far North of Cameroon with a View to Their Incorporation into Polymer Matrices. *Open Journal of Composite Materials*, **16**, 37-58.
https://doi.org/10.4236/ojcm.2026.162003

Received: January 7, 2026
Accepted: February 11, 2026
Published: February 14, 2026

Abstract

This work focuses on microstructural and thermal investigations of *Hyphaene thebaica* fibers. Analyses aimed at understanding their molecular, crystallites, morphological, and thermal behavior are performed in order to control their interactions with polymers. SEM characteristics reveal a crystalline state in the surface areas of the oxidized fibers in particular. The sharp X-ray diffraction (XRD) images are characteristic of cellulose crystals. Fibers retted with water and soda exhibit a crystalline state more than others. This demonstrates the presence of microorganisms acting within the fiber, leaving a certain heterogeneity around these environments caused by these sharp peaks. The vibrational movements observed on the FTIR curves predispose these fibers to physicochemical interactions with organic matter originating from the polymer matrix. Structural infrared analyses revealed the presence of absorption bands concentrated around 1750 cm^{-1} and 1050 cm^{-1} on the DOSO, DOROL, and DOROTER samples, indicating that the treatments eliminated hemicelluloses and some of the lignin. This factor impacts the crystallinity of these fibers and the size of the crystallites they contain. This characteristic suggests good performance in the production of composites with these constituents. Specif-

ically, thermal tests showed an overall mass loss ranging from 5.53% to 74.30%. ADT analysis shows that these fibers begin to degrade under thermal effects at 251˚C for the least resistant and 378˚C for the most resistant. It can be concluded that these fibers can withstand thermocompression and yield structural composites.

Keywords

Hyphaene thebaica Fibers, XRD, FTIR, SEM, TGA/DTA

1. Introduction

Non-renewable subsoil resources have driven scientists to exploit inexhaustible plant matter. Plant fiber-reinforced composite materials [1] are inexpensive in industrial applications as well as in housing and cabinetmaking. These lignocellulosic fibers are readily available and possess exploitable mechanical properties, in addition to their low density. These materials are environmentally friendly and safe for human health compared to conventional synthetic reinforcements. The concept of eco-design, with the development of bio composites [2], is emerging with the creation of composites reinforced with natural fibers [3] [4], whose arrangement within their chosen matrix remains mostly random. The preservation of subsoil resources is pushing researchers and manufacturers to explore plant resources of all kinds. Our immediate environment offers us renewable plant matter. A thorough understanding of their structural essence and their physical, chemical, and thermomechanical performance remains a concern. Hence, our interest in this research. Structural analyses are conducted on lignocellulosic fibers in general [5]. These species are varied in nature. Amorphous fibers can be activated by prior chemical treatment [6] [7]. Others appear more or less crystalline [8] [9]. These chemical treatments are perceived morphologically as an area suitable for chemical activation, facilitated by the removal of lignin and hemicellulose [10]. The enhanced surface becomes a functional site for adsorption and increased binding of functional groups predisposed to receive other chemical groups from various types of matrices. The morphology of biodegradable date palm plant fibers [11], as revealed by scanning electron microscopy, exhibits dimensional variability depending on their origin and bioclimatic environment. Projections regarding the formation of chemical bonds on substrate surfaces are often overlooked. Infrared analyses will allow for the consideration of potential couplings with polymers. Electron transfer at the matrix/fiber interface, similar to what occurs between metals, can also be predicted [12]. The crystalline nature of the fibers obtained after chemical treatment, observed by XRD analysis, has made it possible to identify the adhesion phenomena mentioned above and to evaluate their stiffness and/or flexibility [13]. Studies on the morphological characteristics of plant fibers [14] have shown that these differ depending on the type of treatment ap-

plied [15] [16] to the raw fibers in order to optimize the development of plant-reinforced composites [17]. The physical, thermal, and mechanical properties of plant fibers depend on their ecological zone [18] [19]. *Hyphaene thebaica* fibers from the far north of Cameroon are unexplored yet readily available. The potential for their use as lignocellulosic reinforcement with polymers is explored in this work. Therefore, the intrinsic properties of these *Hyphaene thebaica* species must be understood in this study. Furthermore, these fibers can be subjected to temperature fluctuations. Thermal analyses influencing their physico mechanical behavior will be conducted to optimize the ideal temperature range [20] that these fibers can withstand before considering their incorporation into polymer matrices. All these microstructural and thermal analyses will refine their applications in diverse industrial sectors.

2. Materials and Methods

2.1. *Hyphaene thebaica* Fibers

The four samples that will be the subject of our different analyses are presented in Figure 1.

DIUCHE represents fibers in their natural state; **DOROL** are water-retted fibers; **DOROTER** are underground-retted fibers and **DOSO** are fibers that have undergone treatment with a 1N sodium hydroxide solution in the amount of distilled water used.

Figure 1. DIUCHE (a), DOROL (b), DOROTER (c) and DOSO (d) samples.

2.2. Structural Analysis by X-Ray Diffraction (XRD)

In order to determine structural information for the four fibers, samples studied, an analysis was performed using a Bruker diffractometer with the following characteristics: Cu Kα1 anticathode with wavelength variation at $\lambda = 1.5418$ Å, voltage V = 40 kV, and current I = 30 mA. The angle was used over $6^\circ < 2\theta < 80^\circ$ with steps of 0.02˚ and a time-frequency step of 2 s, in the Bragg-Brentano θ/θ configuration. The maximum intensities of the models used are both qualitative and semi-quantitative [21] [22].

The Crystallinity Index (CI) is obtained using Segal's method according to the relation $CI = (I_{002} - I_{am})/I_{002} \times 100$, where I_{002} is the maximum intensity at the angle 2θ, and I_{am} is the intensity of the amorphous portion. This relation gives the ratio between the crystalline and amorphous phases of the material.

2.3. Analysis by Attenuated Total Reflection Fourier Transform Infrared Spectroscopy (ATR-FTIR)

The chemical bonds and surface functional groups of plant fibers were determined by ATR-FTIR. FTIR spectra were acquired using a Perkin Elmer front-end spectrometer. Data were collected in the Far North region of Cameroon and subjected to instrumentation conditions ranging from 400 to 4000 cm^{-1}, with 16 scans and a resolution of 1 cm^{-1}. All spectra were corrected for background and baseline noise and normalized to the most intense peak. Background spectra were acquired under ambient conditions.

2.4. Morphological Analysis by SEM

The morphology and homogeneity of our DIUCHE, DOROL, DOROTER, and DOSO fiber samples are examined using images obtained with the Zeiss Imager A2M microscopy system, which can produce particles down to 2 µm in size. This Scanning Electron Microscopy (SEM) allows us to observe the surface topography at both the nanoscale and macroscale with high resolution, using the principle of electron-matter interactions. The instrument used (GEMINI model) is coupled to a Zeiss SUPRA 55VP energy-dispersive X-ray spectrometer (EDS).

2.5. Thermogravimetric Analysis (TGA) and Differential Thermal Analysis (DTA)

Thermogravimetric (TGA) and differential thermal analyses were performed using a Perkin Elmer Pyris-1 instrument for these four samples. The tests were carried out on fibrous samples from DIUCHE, DOROL, DOROTER, and DOSO, with a constant heating rate of 10˚C/min up to 1200˚C under nitrogen. This method allowed us to determine mass loss with temperature and to assess the degradation of the fiber structure according to the processing method.

3. Results and Discussion

3.1. XRD Analyses

X-ray diffraction highlights the study of the crystallinity of plant fibers in general. The diagrams used for the four *Hyphaene thebaica* fiber samples show reduced interval curves between $2\theta = 5$ and 40˚. The peaks generated by these samples appear to originate from cellulose crystals [23]. This characteristic jointly assesses the fiber stiffness and its crystallinity index (CI) while specifying the characteristic phases [24] on the diffractograms (**Figure 2**). All four diffractograms show at least three reflections with a major one, characteristic of natural fibers. Around $2\theta =$ 22.30˚ with minor variances, the four samples exhibit a very intense major peak corresponding to the cellulose crystallographic plane at (002). Around $2\theta = 35$˚, it is a slight bump belonging to the crystallographic plane (040); the amorphous zone of cellulose emerges from it for these samples [25] [26]. Specifically, the most

prominent peak is that of DOROL extracted with water. It appears more crystalline due to the maceration process combined with the action of ions from water molecules. This peak is followed by that of DOSO fibers extracted from an alkaline medium. The same is true for those extracted underground, namely DOROTER. An interpretation emerges from these three samples: the presence of microorganisms acting within the plant, leaving a certain heterogeneity around these media (see SEM), explaining these sharp peaks. These samples nevertheless exhibit an amorphous zone around $2\theta = 16.49^{\circ}$ close to the (110) lattice of the crystallographic plane. This gives them the amorphous behavior of cellulose, hemicellulose, pectin, and lignin [27]. DOROL also exhibits the second largest peak in this sample, although it appears as a bump. This explains its amorphous behavior. However, around $2\theta = 11.12^{\circ}$, the elimination of amorphous constituents occurs, thus promoting an increase in cellulose crystallinity. This is a significant advantage for predicting the physico-mechanical properties of the composites to be formed there. Due to their similarity to the other three samples, this behavior can be attributed to them. However, the DIUCHE sample appears more amorphous with a boss around $2\theta = 22.38^{\circ}$. This is confirmed by its crystallinity index of 43.61%. In contrast, the DOROTER samples are strongly influenced by the soil environment, which could be alkaline or alkaline-earth. Its crystallinity has been affected by ions from minerals; hence, there are mitigable characteristics. The DOSO sample seems to perform well with a crystallinity rate of 66.07%, higher than the other samples. This is explained by the fact that all the characteristic peaks of its curve are sharp. This also predisposes them to good interfacial adhesion in the fabrication of composite materials, especially with polymers. This confirms the crystalline nature of these fibers overall [28].

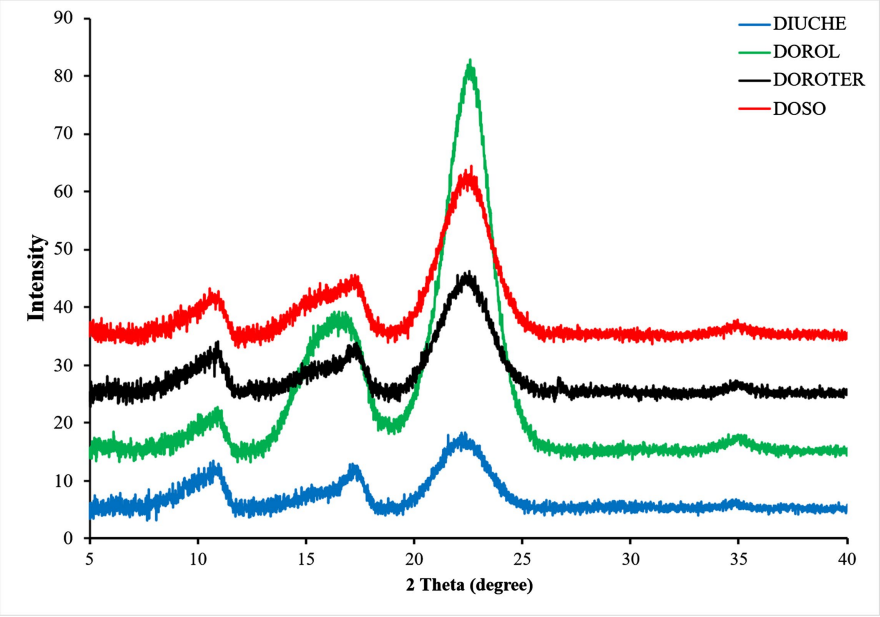

Figure 2. XRD of the four samples.

3.2. FTIR Analysis

The FTIR curves of the four samples DIUCHE, DOROL, DOROTER, and DOSO show similarities along the spectra, with some disparities. This is explained by variances arising from the different extraction techniques used for these fibers. The similarity is already apparent in the common presence of cellulose, hemicellulose, and lignin. Thus, the broad band appearing in the 3200 - 3600 cm^{-1} region is primarily attributed to hydroxyl groups [29] [30]. This area of peaking marks the increase in hydroxyl groups in the cellulose of the samples [31]. Specifically, around 3350 cm^{-1}, the alcohol group forms at the expense of the OH group of the hemicellulose components. The peak wavelength around 2900 cm^{-1} is characteristic of plant fibers and corresponds to the stretching vibration of the aliphatic CH group. The small peak at 2839 cm^{-1} belongs jointly to the DIUCHE and DOROL fibers and is specific to the symmetric and asymmetric C-H stretching vibrations in CH, CH_2, and CH_3 groups of plants. [32] The peak at 1718 cm^{-1} is attributed to the C=O group of cellulose and hemicellulose. This is common to the DIUCHE, DOROTER, and DOROL samples. The absence of this peak in the DOSO sample is explained by the structural modification undergone by its extraction method. A slight peak can be observed around 1510 cm^{-1}, which shows the rigid character of all these fibers, favorable to the C=C bonds of the lignin aromatic ring. [33] The peak at 1433 cm^{-1} is attributed to the CH_2 group of these four samples. The multiple sawtooth peaks in the 1200 - 1400 cm^{-1} range are comparable to the C-O bonds of the aliphatic hemicellulose ring and the C-OCH bonds of cellulose [34]. The intensity of the bands around 1015 cm^{-1} is attributed to the C-O and C=O stretching of cellulose on the one hand, and to that of hemicelluloses and lignin on the other [35]. Generally, it can happen that the bands disappear after treatment with an alkali. This is the case for the absorption band of the carbonyl group C=O at 1712 cm^{-1}, which disappears for the DOSO sample [27], indicating that this band belongs to a hemicellulose component [6]. This is why hemicellulose is considered the main component affected by structural modification during the dissolution of fibers by alkaline solutions [36]. The small peak at 873 cm^{-1} corresponds to glycosidic vibrations of hemicellulose. The flattening of some DOSO peaks is explained by the surface modification of the fibers dissolved by the alkaline solution. Hemicellulose is the compound most affected by this modification, although it is also noticeable in lignin. The weak peaks around 1140 to 1200 cm^{-1} are attributed to elongations of the C-O-C ether groups of cellulose and hemicellulose. The acute peaks at 1050 cm^{-1} are those of the characteristic bands of the stretching vibrations of the C-O groups of the cellulose contained in the four samples [37]. Main peaks are recorded in **Table 1** below.

For comparison, it is important to note the impact of the extraction method on these fibers. Immersion of these fibers in an alkaline medium decreased the density of observable vibrational movements by reducing either the width of the peaks or by their disappearance. The same is true for the sequestration of these fibers underground. Indeed, the presence of subsurface microorganisms contributed to

the removal of physicochemical substances from these fibers. This is visible on the DOROTER infrared curve; its peaks are much softer than those of DIUCHE and DOROL. Since the reference curve is that of DIUCHE, which underwent no treatment, a certain similarity in shape is observed compared to DOROL, with sharper peaks in the latter case. This demonstrates the action of ions contained in water molecules in promoting and participating in vibrational movements during subsequent chemical bonding, unlike DOSO and DOROTER fibers.

Table 1. Main peaks of the infrared curves of the four samples [31] [38]-[41].

Wavenumber [cm^{-1}]	Peak description	Nature of connection
3500 - 3150	(Bump (broad peak)	Characteristic of hydrogen -OH bonds.
2839	Medium peak	Symmetric and asymmetric CH stretching vibrations in CH group.
2900	Small peak	Symmetric and asymmetric CH stretching vibrations in CH_2 and CH_3 groups.
1718	Sharp peak	C=O grouping of cellulose and hemicellulose.
1643	Sharp peak	1643 cm^{-1} is assigned to H-O-H bending of absorbed water.
1590	Sharp peak	Symmetric C=C elongation of the aromatic ring in lignin components.
1049	Strong band with medium peaks for all four samples	attributed to C-O stretching in cellulose, hemicelluloses, and lignin or C-O-C stretching in cellulose and hemicelluloses.
1520, 1447 and 1335		corresponds to the aromatic skeletal vibrations and ring breathing with C-O stretching of the lignin components of *Hyphaene thebaica* various fibers species.
1733		band of the carbonyl stretching absorption of ester and carboxyl groups, which are the most abundant in *Hyphaene thebaica* hemicelluloses.
1248 - 1059		The band in the region of 1248 - 1059 cm^{-1} involves the C-O stretching vibrations of the aliphatic primary and secondary alcohols in the cellulose, hemicellulose and lignin.

The similarities in the FT-IR characteristics can be attributed to the main components of various fiber species (**Figure 3**), namely cellulose, hemicellulose, and lignin. Comparing all the spectra at different locations and positions across all species, the peaks at frequencies of 3410 and 1051 cm^{-1} are the dominant spectral feature. The strength and width of the band at 3410 cm^{-1} originate from OH stretching. In contrast, the sharp and intense band at 1049 cm^{-1} is attributed to C-O stretching of cellulose, hemicelluloses, and lignin, followed by C-O-C stretching of cellulose and hemicelluloses. Similarly, the intense band at 1643 cm^{-1} is attributed to H-O-H bending of absorbed water. The absorbances at 1520, 1447, and 1335 cm^{-1} correspond to aromatic vibrations of the skeleton and to ring respiration with C-O stretching of lignin components in various species of these fibers. The distinct band observed at 1733 cm^{-1} is due to absorption of carbonyl stretching of ester and carboxyl groups, which are most abundant in hemicelluloses. The

band between 1248 and 1059 cm^{-1} involves C-O stretch vibrations of primary and secondary aliphatic alcohols in cellulose, hemicellulose, and lignin. Previous studies have shown that lignocellulosic fibers can undergo significant weight loss due to the partial dissolution of hemicelluloses, lignin, and pectin when treated with alkali. The C=O absorption band of the carbonyl group at 1733 cm^{-1} disappears upon alkali treatment of natural fibers, proving that this band is due to the hemicellulose component of the natural fibers. A small, distinct band at 903 cm^{-1} results from α-carbohydrate bonds between the sugar units of hemicelluloses and celluloses.

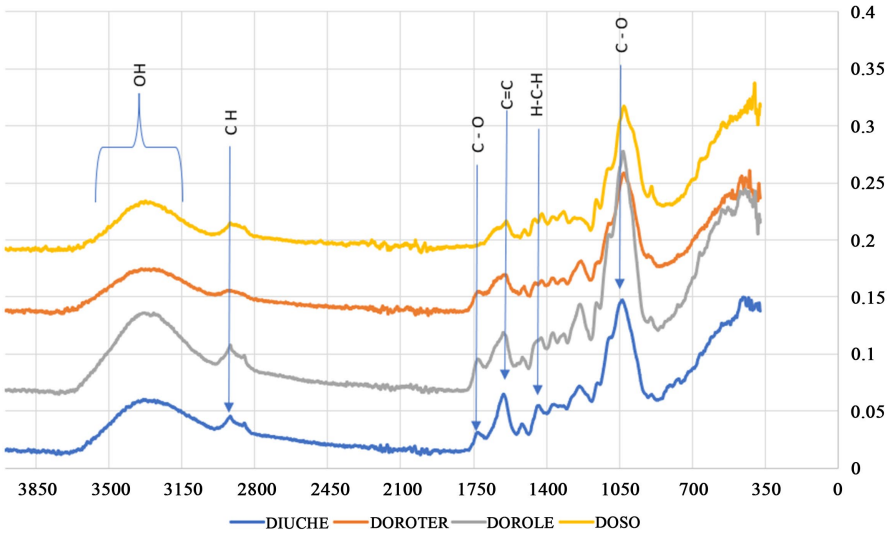

Figure 3. Infrared curves of the four samples.

3.3. Morphological Interpretation

Figures 4-7 present samples with varied appearances depending on whether the fibers are raw or have undergone different retting techniques. The DIUCHE fiber samples (Figures 4(a)-(d)) exhibit a very uneven topography, marked by undulations and hollows resembling crocodile skin. This configuration does not offer perfect homogeneity in the distribution of the resin layer. This impacts the formation of interfacial bonds between this fiber and its resin matrix. Cohesion at the interface and the interphase will not have the same mechanical performance. Indeed, shear stresses, which act as pull-out forces, will facilitate decohesion.

Initially, water retting preserves the fiber configuration and microfibrils by maintaining their interlocking, lamellar arrangement (Figure 4(a), Figure 4(b)) when they remain bound together. As the extraction process continues, the fibers separate (Figure 4(c), Figure 4(d)). An improvement in roughness is observed with the progressive disappearance of surface residues, the cause of the undulations seen in raw fibers. It is certain that the ions present in water molecules create molecular interactions with essential components of the intrinsic constituents of cellulose. Underground retting is characterized by the presence of mineral matter. The various rinsing processes had a significant impact on the fibers. Indeed, the

runoff of powdery material from the ground facilitated the removal of microfibrils to the surface. This explains why the surface of the fibers in Figures 5(a)-(c) appears less uneven than those of DIUCHE and DOROL. Concave topography is less noticeable in this case. This suggests a fairly homogeneous resin formulation on the fiber, which will result in good arrangement and efficient transmission of residual stresses from one fiber to another. This will create a perfectly continuous medium where the constitutive laws of continuum mechanics would find a perfect model.

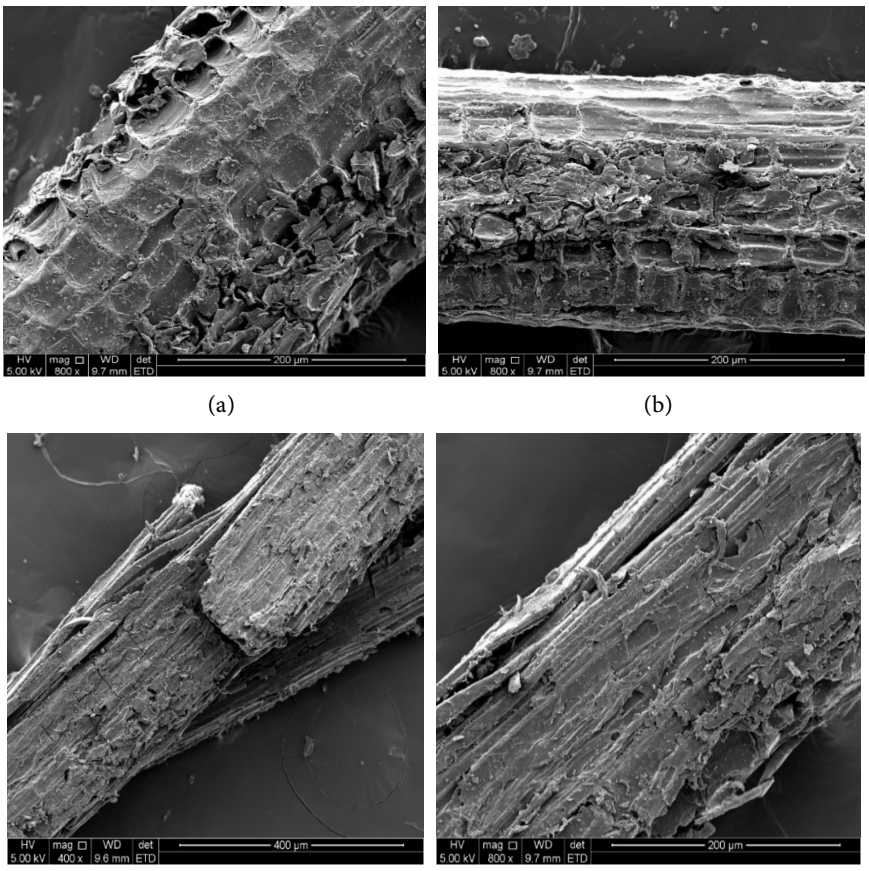

(a) (b)

(c) (d)

Figure 4. DIUCHE fibers at various magnifications.

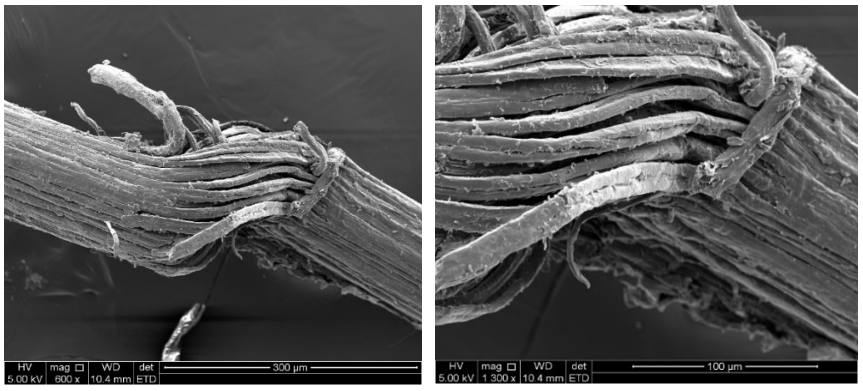

(a) (b)

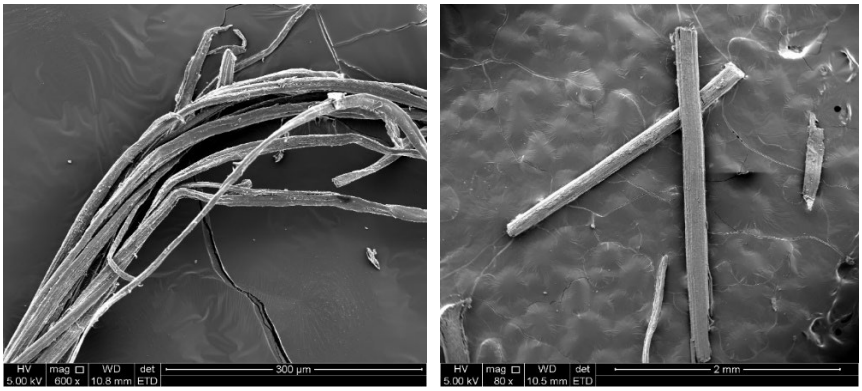

(c) (d)

Figure 5. DOROL fibers at various magnifications.

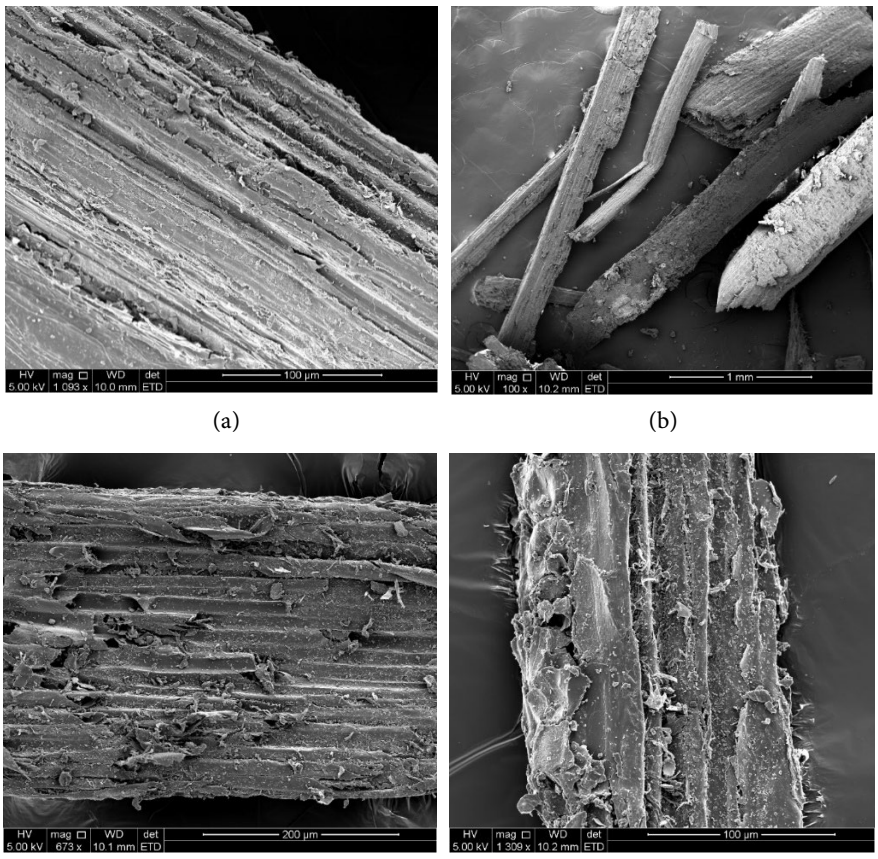

(a) (b)

(c) (d)

Figure 6. DOROTER fibers at various magnifications.

The alkaline environment brought about a change both visually and morphologically. Retting with soda made the fibers lighter and cleaner. Indeed, the surface impurities in the form of microfibrils were cleaned thanks to the presence of sodium hydroxide. These impurities are primarily composed of lignins and hemicelluloses. The latter are, in most cases, responsible for the amorphous character of these fibers observed in XRD curves. The high cellulose content in these *Hy-*

phaene thebaica fibers has revealed their intrinsic configuration. Therefore, morphologically, the concave shapes and multiple microbumps have undergone a kind of leveling, but with many suspended fibrillar particles that serve to accommodate resin runoff and fill areas of increased concavity. The interfacial medium is thus rendered much more linear (**Figure 7(a)**, **Figure 7(b)**), and the density of the constituents is made more homogeneous.

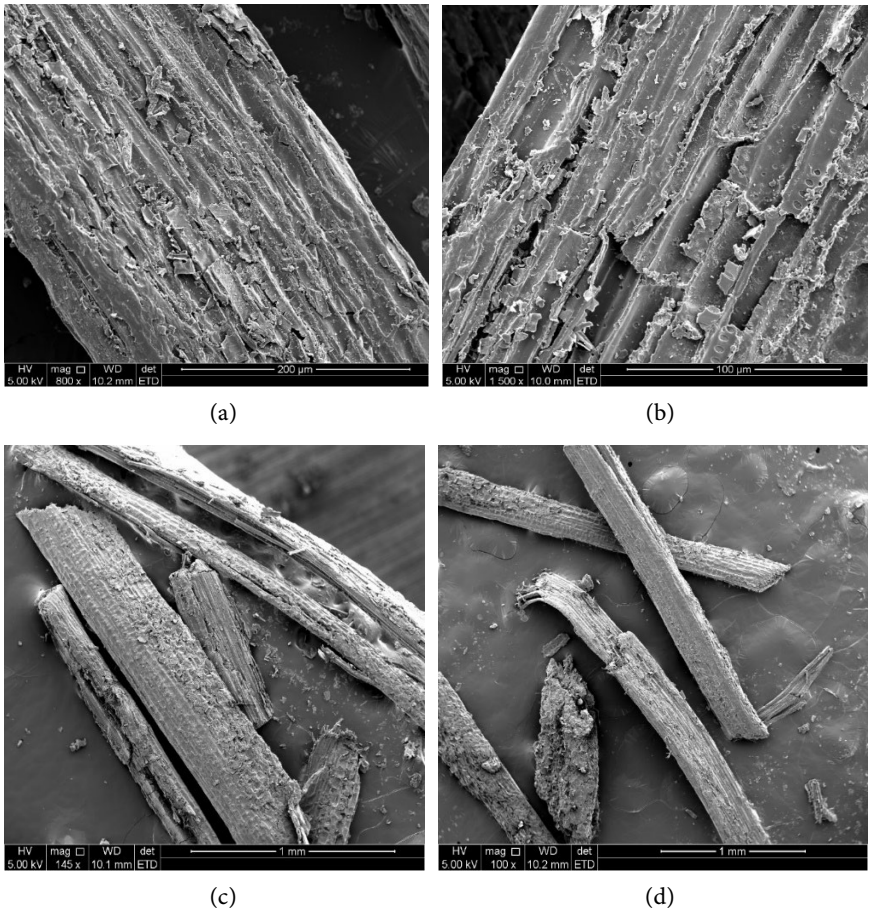

(a) (b)

(c) (d)

Figure 7. DOSO fibers at various magnifications.

DIUCHE's SEM images show a medium of fibers with a highly diverse topography. This medium reveals the presence of hemicelluloses and lignin, responsible for the amorphous character of the microfibrillar areas. This is due to the presence of impurities and voids in the form of hollows on the surface of the fibers. Furthermore, these contaminants facilitate the separation of the fibers from the matrix. These impurities were eliminated during the retting process, which acts as a treatment, destroying the lignin to promote adhesion between the constituents [42]. Its XRD curve perfectly illustrates this. Unlike the DIUCHE fibers, the other three appear to exhibit a flatness characteristic of the high cellulose content after retting. This flatness is an interfacial zone conducive to the formation of chemical bonds between the matrix resin and the reinforcing fibers. Water retting releases both hydronium and hydroxide ions. The latter combine with compatible ions from the

resin. The thickness of this zone of molecular interactions determines the type of mechanical bonds due to the potential long molecular chain and the duplication of functional groups, which is responsible for bond formation and the mechanical performance of the resulting composite material. The same will be true for underground retting, where ions from the water will be replaced by ions from silicates or other ions resulting from the geochemistry of the soil present. All of these will contribute to obtaining composite materials for structural applications in industrial engineering. In the latter case, the ions released by the caustic soda and the essential oils of the cellulose in the studied fibers will chemically combine with the type of resin used. In this particular case, SEM shows us that there will be a good interphase layer where the interfacial manifestation of all the chemical-mechanical bonds will be evident. These cavities significantly reduce the mechanical performance of the fibers, with a surface morphology that does not promote consolidation mechanisms at the fiber-resin interface. The influence of retting, which provides a surface treatment, facilitates the separation of microfibrils with the elimination of lignin and release of the fiber-matrix adhesion field through the mobilization of functional groups, thus ensuring better composite consolidation.

Access to the surface biochemical composition of the fibers would allow for a significant advance in understanding adhesion mechanisms using the chemical bonding model. In this study, where the two fibers are of different natures, surface roughness is a parameter to consider, and the mechanical anchoring model should be coupled with the chemical bonding model. The high adhesion value for the hemp/epoxy system supports the use of these fibers in composites. Although the performance of hemp fibers is lower than that of flax fibers, their price is lower and more stable over the years.

3.4. Thermal Analyses

Figures 8-11 present the thermogravimetric analysis (TGA) curves and their derivatives on the four *Hyphaene thebaica* fiber samples. DIUCHE, DOROL, DOROTER and DOSO fibers show similarities in the different phases of thermal transformations, with some disparities depending on the treatment method.

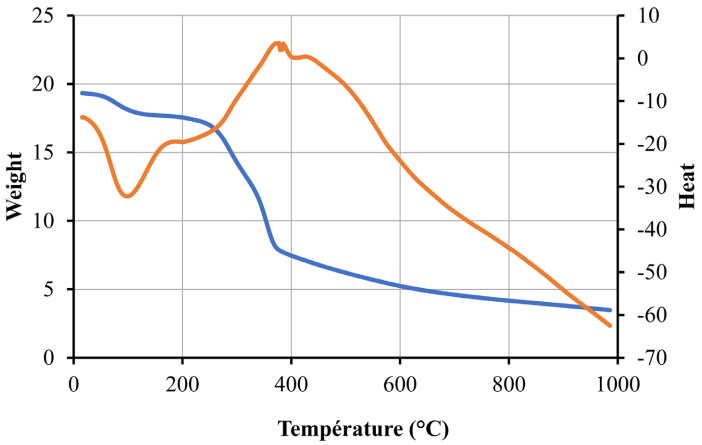

Figure 8. DIUCHE TGA/DTA curves.

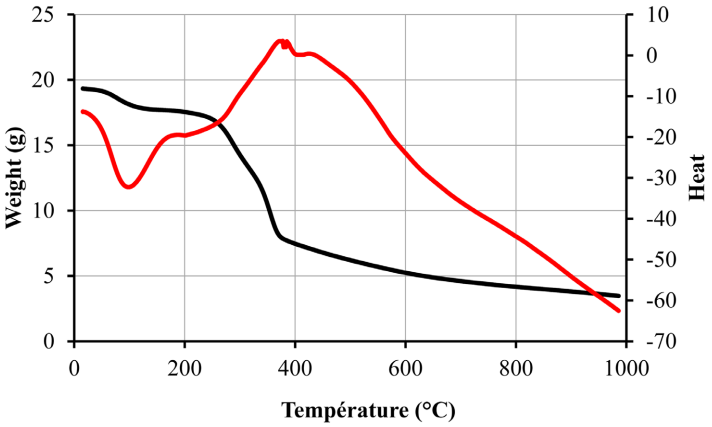

Figure 9. DOROL TGA/DTA curves.

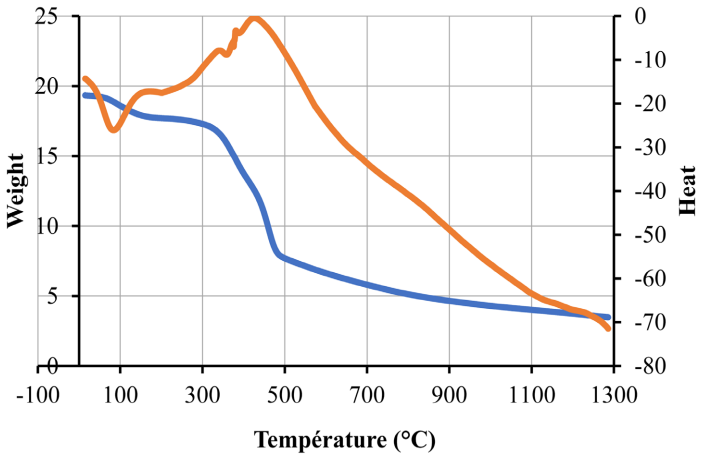

Figure 10. DOROTER TGA/DTA curves.

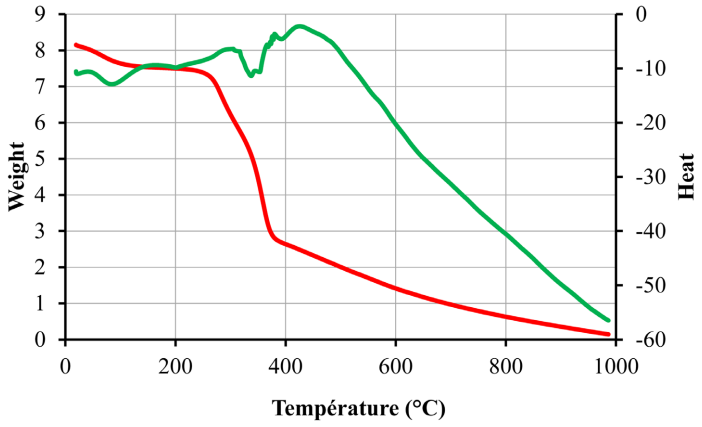

Figure 11. DOSO TGA/DTA curves.

The DIUCHE figure presents four phases of thermal degradation. The initial phase occurs between 15˚C and 104˚C with a mass loss of 6.77%. It is represented on the DTG curve by the first endothermic peak at this same temperature. This first change in the DTG curve is characterized by a rapid, linear descent followed

by a rise, leaving a somewhat sharp peak. This morphological characteristic of the curve reflects the first structural change in the DIUCHE fibers. This transformation remains minimal, as these fibers still retain 93.22% of their major constituents. This low percentage is generally attributed to the removal of existing moisture due to the hydrophilic nature of lignocellulosic materials [43] and the removal of any impurities present in surface areas of these fibers [44] [45]. The second phase corresponds to the highest mass loss for these DIUCHE samples. It is estimated at 59.46% at a temperature of 378˚C. Only 40.53% of essential constituents remain. These values are reflected on the curve in **Figure 8** by a sharp drop in the TGA curve and a sharp rise in the DTA curve, marked by an exothermic peak.

It is noteworthy that the temperature range varies from 378˚C to 382˚C, with an exothermic peak exhibiting a zigzag pattern in 0.19 seconds. This extremely short time interval demonstrates the abrupt decline of these fibers at this temperature. They continued to resist up to 390˚C; beyond this point, the conjugate curves asymptotically approach their final melting point. Indeed, at the microstructural level, this mass loss is accompanied by the destruction of the cellulose constituents. The significant change in concavity around 363˚C marks the beginning of the structural decomposition of hemicellulose, which is followed by the onset of cellulose decomposition. This phase is one of the most important, as it is here that all the thermal resilience is observed. This also explains the greatest mass loss, at 51.69%. The onset of cellulose decomposition corresponds to a temperature of 390.32˚C with a mass loss of 1.73%. Above this temperature, total decomposition of all constituents occurs, marked by the melting of the fibers.

The DOROL samples share similarities with those from DIUCHE, as shown in the configuration of the two figures. However, differences are observed in the structural transformations, as evidenced by peaks in the DTG curves. The first endothermic peak of the DTG curve appears as a bump at 83.15˚C. This explains the shallow slope of the TGA curve for this temperature range, where a low mass loss of 4.89% is recorded. The second phase is characterized by a long thermal resistance duration, approximately 6.63 seconds at 251.89˚C. Despite this considerable time, the fibers retain their essential properties. From 251.89˚C to 328.55˚C, a significant mass loss of approximately 34.28% occurs, with an exothermic peak exhibiting a zigzag pattern on the DTG curve. This zigzag-shaped animation shows the fiber's final resilience strength. This phase is also marked by a significant drop in the TGA curve. Above 328.55˚C, a renewed crystallization is visible as a slight exothermic peak around 422.20˚C. This final phase is marked by a mass loss of approximately 32.22%. It is beyond this temperature that the two curves asymptotically slope downwards, indicating the progressive transformation of the fiber into ash. This is why the two conjugate curves asymptotically converge in the same direction.

Fibers oxidized underground also exhibit the four phases of thermal degradation, as in the two previous cases. These fibers have been influenced by the organic and mineral matter of the soil used. The first thermal transformation occurs at

88.80˚C with a slight inverted hump, resulting in a mass loss of approximately 6.52% (**Figure 10**). This phase is linked to the elimination of water molecules from the fiber's moisture content. The second phase, more extensive due to its thermal stability, begins to transform at 344.85˚C. It is characterized by a small exothermic peak that causes a sharp drop in the TGA curve with a mass loss of 46.61%. Several structural transformations influence the intrinsic properties of the fiber. It should be noted that the fiber withstood temperatures up to 254.51˚C without mass loss. Between 344.85 and 359.67˚C, the fiber continues to lose mass progressively, despite the presence of zigzag-shaped artifacts. Above 427.93˚C, the fiber enters the final degradation phase of deterioration. The two curves converge asymptotically towards the same trajectory. It is observed that these fibers, oxidized underground, retain their stiffness [46] [47] up to a temperature of 290.27˚C, at which point the fiber has lost all of its lignin.

The thermograms of the DOSO samples show mass loss trends similar to previous ones. The TGA curves show three phases in the evolution of its pyrolysis. The first phase is almost endothermic (DTA curve) with a low concavity peak at a temperature of 86.33˚C. This corresponds to a mass loss of 5.533%, meaning that 94.47% of the constituents remain intact. A shallow slope of the TGA curve is observed, characteristic of this low pyrolysis rate. The second mass loss phase is observed at a temperature of 294.26˚C. A double slope is observed at different gradients. The first slope of the TGA curve for this phase registers 21.72%, and the second reaches 38.61% at a temperature of 339.26˚C. At this temperature, the fibers still retain 61.39% of their intrinsic constituents. A resurgence of thermal resistance is visible on the DTA curve with an endothermic peak followed by a recrystallization phase up to 434.02˚C. At this temperature, the DOSO fiber loses more than 70% of its constituents and begins its structural loss where no internal reorganization is observable. The mass loss observed around 86.33˚C is attributable to fiber dehydration [48], the removal of volatile surface compounds [46], and lignin deterioration [49].

This second, exothermic phase corresponds to the pyrolytic decomposition and oxidation of the dry plant material. During this phase, low molecular weight volatile products are permanently released [50].

The temperature range of the second phase (251˚C - 378˚C) corresponds to the destruction of hemicellulose, cellulose, pectin, and a portion of the lignin. The degradation temperatures of hemicellulose and cellulose range from 320˚C to 360˚C, while the degradation temperature of lignin is around 400˚C [48]. Studies on wood pyrolysis [50] in general show that hemicellulose decomposition occurs at 320˚C. However, DOSO fibers appear to retain their structure at 339.26˚C. The structural decomposition of cellulose occurs at 434.02˚C, while that of lignin is progressive, starting at 294.36˚C and reaching a total melting point exceeding 900˚C. The final phase, ranging from 339.26˚C to 900˚C for these samples, marks the melting of the organic matter, which is progressively transformed into carbonized products. This corresponds to the pyrolytic degradation initiated during

the second phase. The two curves, TGA and DTA, converge linearly towards the same asymptotic branch.

Thus, the destruction of most of the structural elements and their reorganization for the formation of other chemical bonds, such as the aromatic cyclization of carbon residues [32] [36], are reflected in the exothermic peaks of the DTA curve. The main degradation of the DOSO fibers occurs at a temperature above 394.06˚C. The results obtained are comparable to those reported in the literature [52]-[54]. Table II.6 shows the different degradation temperatures obtained for the fibers before and after treatment, as well as the mass loss of the sample at the end of the experiment.

Table 2 above summarizes the major variations in phase changes under thermal influence. It is clear that the temperature range [83˚C; 104˚C] corresponds to a very low mass loss due solely to the evaporation of water present in the fibers for the four samples studied. This is normal behavior for these fibers due to their initial crystallization. The best behavior at this stage is water retting, followed by caustic soda retting, and finally underground retting. This confirms the results obtained by XRD [55]. The second phase corresponds to the structural decomposition of the microfibrils. It ranges from 250˚C to 378˚C. The DOROL samples begin their decomposition at 251.89˚C, followed by the DOSO samples at 294.36˚C, then the DOROTER samples at 344.85˚C, and finally the DIUCHE samples at 378.27˚C. It should be noted that this phase is characterized by the thermal resistance of these fibers. This resilience is observed on the various TGA curves by the almost horizontal portion. The decay is observable on the differential DTA curves with exothermic peaks or slight bumps on the four thermal figures. Mass losses with the associated temperatures are recorded in **Table 2**. These exothermic peaks mark the degradation of cellulose and lignin [56] at these temperature ranges. The treated fibers generally exhibit better performance in terms of thermal resistance. DOSO (296.06˚C) is more resistant than DOROTER (291.64˚C), which in turn surpasses DOROL (287.31˚C). It is clear that the treatment applied to the *Hyphaene thebaica* fibers improves their thermal stability. This confirms previous results on the degradation of plant fibers [57] with temperature changes. The third column of **Table 2** shows the ultimate resistance temperatures of each of these samples, because beyond these temperatures, structural deterioration begins in each one. This final stage can be attributed to the decomposition of the carbon skeleton within the structure of each sample [58]. The zigzag patterns on the four curves indicate the breakdown of glycosidic bonds in cellulose and any decomposition of lignin. hence the prediction of their behavior in structural composite materials. For comparison, DIUCHE and DOROL share similarities, which can be explained by the fact that water retting did not denature the raw DIUCHE fibers. The few observed differences likely stem from excess hydronium and hydroxide ions produced by the water molecules. The decline temperature of DIUCHE is 390.22˚C, while that of DOROL is 422.20˚C. The decline temperatures of DOROTER and DOSO are 430˚C and 434˚C, respectively. The presence of zigzags

demonstrates the resilience of these fibers up to a temperature of at least 328˚C for the DOROL sample, which appears to be the least resistant, and up to 382˚C for DIUCHE, the most resistant. Overall, the degradation phases begin with the drying of the fiber, characterized by a slight loss of mass. Next comes the degradation of hemicelluloses, followed by that of celluloses. This is characterized by a slight change in the slope of the TGA curve. Finally, the degradation of lignin occurs.

Table 2. Degradation temperatures and their mass loss.

	T_1 (˚C)	T_2 (˚C)	T_3 (˚C)	T_4 (˚C)
DIUCHE	104˚C (6.77%)	378˚C (59.46%)	382.67˚C (59.92%)	390.32˚C 60.65%)0
DOROL	83.15˚C (4.89%)	251.89˚C (34.37%)	328.55˚C (65.91%)	422.20˚C (67.73%)
DOROTER	88.80˚C (6.51%)	344.85˚C (46.61%)	359.67˚C (60.49%)	430.72˚C (74.30%)
DOSO	86.33˚C (5.53%)	294.36˚C (21.72%)	339.26˚C (38.61%)	434.02˚C (70.46%)

T1: Temperature at the onset of degradation; T2: Temperature of first structural modification; T3: Crystallization temperature; T4: Maximum degradation temperature; P: Mass loss rate. Each temperature range is accompanied by its mass loss in parentheses.

Structural disintegration under the effect of temperature is demonstrated by these analyses. Below 90˚C on average, *Hyphaene thebaica* fibers retain a large quantity of their chemical and organic resources; consequently, they still possess their resilience capacity. The shallow slope observed on the TGA curve predisposes the material to a resilient character tending towards a behavior close to ductility. It should therefore be emphasized that all these fibers embedded in a polymer matrix will exhibit even better thermal behavior in terms of resistance.

4. Conclusion

Investigations into the microstructural properties of *Hyphaene thebaica* palm fibers are conducted through analyses aimed at understanding their molecular, crystallites, morphological, and thermal behavior. This aims to control their combinations with polymers and to predict their physical and mechanical properties within composites. The compatibility between lamellar microfibrils and others, exhibiting varying concavity roughness accompanied by bosses, will be achieved with the presence of polymers. These SEM characteristics suggest a crystalline state on the surface areas of the retted fibers in particular. Sharp peaks in XRD are characteristic of cellulose crystals. Fibers retted with water and sodium hydroxide exhibit a more crystalline state than the others. This demonstrates the presence of microorganisms acting within the fiber, leaving a certain heterogeneity around

these environments, which explains these sharp peaks. The vibrational movements observed on the FTIR curves predispose these fibers to physicochemical interactions with organic matter from the polymer matrix. Structural infrared analyses showed the presence of absorption bands concentrated around 1750 cm^{-1} and 1050 cm^{-1} on the DOSO, DOROL, and DOROTER samples; this indicates that the treatments eliminated hemicelluloses and some of the lignin. This factor impacts the crystallinity of these fibers and the size of the crystallites they contain. This characteristic suggests good performance in the production of composites using these constituents, because it is a theoretical prediction based on fiber characterization. Specifically, thermal tests showed an overall mass loss ranging from 5.53% to 74.30%. ADT analysis shows that these fibers begin to degrade under thermal effects at temperatures ranging from 251˚C for the least resistant to 378˚C for the most resistant. It can be concluded that these fibers can withstand thermocompression in the production of fiberboard panels.

Conflicts of Interest

The authors declare no conflicts of interest regarding the publication of this paper.

References

[1] Terzopoulou, Z.N., Papageorgiou, G.Z., Papadopoulou, E., Athanassiadou, E., Alexopoulou, E. and Bikiaris, D.N. (2015) Green Composites Prepared from Aliphatic Polyesters and Bast Fibers. *Industrial Crops and Products*, **68**, 60-79. https://doi.org/10.1016/j.indcrop.2014.08.034

[2] Ramesh, P., Prasad, B.D. and Narayana, K.L. (2019). Morphological and Mechanical Properties of Treated Kenaf Fiber/MMT Clay Reinforced PLA Hybrid Biocomposites. *AIP Conference Proceedings*, **2057**, Article ID: 020035. https://doi.org/10.1063/1.5085606

[3] Arpitha, G.R. and Yogesha, B. (2017) An Overview on Mechanical Property Evaluation of Natural Fiber Reinforced Polymers. *Materials Today*: *Proceedings*, **4**, 2755-2760. https://doi.org/10.1016/j.matpr.2017.02.153

[4] Essabir, H., Bensalah, M.O., Rodrigue, D., Bouhfid, R. and Qaiss, A. (2016) Structural, Mechanical and Thermal Properties of Bio-Based Hybrid Composites from Waste Coir Residues: Fibers and Shell Particles. *Mechanics of Materials*, **93**, 134-144. https://doi.org/10.1016/j.mechmat.2015.10.018

[5] Awad, S., Zhou, Y., Katsou, E., Li, Y. and Fan, M. (2020) A Critical Review on Date Palm Tree (*Phoenix dactylifera* L.) Fibres and Their Uses in Bio-Composites. *Waste and Biomass Valorization*, **12**, 2853-2887. https://doi.org/10.1007/s12649-020-01105-2

[6] Kabir, M.M., Wang, H., Lau, K.T. and Cardona, F. (2012) Chemical Treatments on Plant-Based Natural Fibre Reinforced Polymer Composites: An Overview. *Composites Part B*: *Engineering*, **43**, 2883-2892. https://doi.org/10.1016/j.compositesb.2012.04.053

[7] Bezazi, A., Amroune, S. and Scarpa, F. (2015) Statistical Analysis and Effect of Chemical Treatments on the Physico-Mechanical Behavior of Date Palm Cluster Arm Fibers. *Scientific and Technical Review*, **31**, 108-120.

[8] Abu-Thabit, N.Y., Judeh, A.A., Hakeem, A.S., Ul-Hamid, A., Umar, Y. and Ahmad, A. (2020) Isolation and Characterization of Microcrystalline Cellulose from Date Seeds (*Phoenix dactylifera* L.). *International Journal of Biological Macromolecules*, **155**, 730-739. https://doi.org/10.1016/j.ijbiomac.2020.03.255

[9] Trache, D., Hussin, M.H., Hui Chuin, C.T., Sabar, S., Fazita, M.R.N., Taiwo, O.F.A., *et al.* (2016) Microcrystalline Cellulose: Isolation, Characterization and Bio-Composites Application—A Review. *International Journal of Biological Macromolecules*, **93**, 789-804. https://doi.org/10.1016/j.ijbiomac.2016.09.056

[10] Mahmoudi, K., Hamdi, N. and Srasra, E. (2014) Preparation and Characterization of Activated Carbon from Date Pits by Chemical Activation with Zinc Chloride for Methyl Orange Adsorption. *Journal of Materials and Environmental Science*, **5**, 1758-1769.

[11] Essabir, H., El Achaby, M., Hilali, E.M., Bouhfid, R. and Qaiss, A. (2015) Morphological, Structural, Thermal and Tensile Properties of High Density Polyethylene Composites Reinforced with Treated Argan Nut Shell Particles. *Journal of Bionic Engineering*, **12**, 129-141. https://doi.org/10.1016/s1672-6529(14)60107-4

[12] Kinloch, A.J. (1980) The Science of Adhesion. *Journal of Materials Science*, **15**, 2141-2166. https://doi.org/10.1007/bf00552302

[13] Tserki, V., Panayiotou, C. and Zafeiropoulos, N.E. (2005) A Study of the Effect of Acetylation and Propionylation on the Interface of Natural Fibre Biodegradable Composites. *Advanced Composites Letters*, **14**, 65-71. https://doi.org/10.1177/096369350501400202

[14] AL-Oqla, F.M., Hayajneh, M.T. and Al-Shrida, M.M. (2022) Mechanical Performance, Thermal Stability and Morphological Analysis of Date Palm Fiber Reinforced Polypropylene Composites toward Functional Bio-Products. *Cellulose*, **29**, 3293-3309. https://doi.org/10.1007/s10570-022-04498-6

[15] Boussehel, H., Ghelani, L., Guerira, B., Bezazi, A., Reis, P.N.B., Alothman, O.Y., *et al.* (2025) Effect of Treatment on Mechanical and Thermal Properties of Date Palm Fibers/Polyvinyl Chloride Composites. *Journal of Vinyl and Additive Technology*, **31**, 604-621. https://doi.org/10.1002/vnl.22194

[16] Maache, M., Bezazi, A., Amroune, S., Scarpa, F. and Dufresne, A. (2017) Characterization of a Novel Natural Cellulosic Fiber from *Juncus effusus* L. *Carbohydrate Polymers*, **171**, 163-172. https://doi.org/10.1016/j.carbpol.2017.04.096

[17] Bruzzese, C. (2023) Composites and Active Materials: Use of Lignocellulosic Fibers for the Development of Bio-Based Products. Ph.D. Thesis, Université Grenoble Alpes. https://theses.hal.science/tel-04226047v1

[18] Alshahrani, H., Alshammari, B.A., Shah, A.H. and Dayo, A.Q. (2022) Development of Hybrid Composite Utilizing Micro-Cellulose Fibers Extracted from Date Palm Rachis in the Najran Region. *Polymers*, **14**, Article 4687. https://doi.org/10.3390/polym14214687

[19] Nouar, Y., Nekkaa, S., Fernández-García, M. and López, D. (2018) The Thermal and Thermomechanical Behaviors of Spartium junceum Flour Reinforced Polypropylene Composites: Effects of Treatment and Flour Content. *Composite Interfaces*, **25**, 1067-1089. https://doi.org/10.1080/09276440.2018.1459126

[20] Beroual, M., Trache, D., Mehelli, O., Boumaza, L., Tarchoun, A.F., Derradji, M., *et al.* (2020) Effect of the Delignification Process on the Physicochemical Properties and Thermal Stability of Microcrystalline Cellulose Extracted from Date Palm Fronds. *Waste and Biomass Valorization*, **12**, 2779-2793. https://doi.org/10.1007/s12649-020-01198-9

[21] Cook, H.E., Johnson, P.D., Matti, J.C. and Zemmels, I. (1975) Methods of Sample Preparation and X-Ray Diffraction Data Analysis, X-Ray Mineralogy Laboratory, Deep Sea Drilling Project, University of California, Riverside. In: Kaneps, A.G., *et al.*, Eds., *Initial Reports of the Deep Sea Drilling Project*, U.S. Government Printing Office, 999-1007. https://doi.org/10.2973/dsdp.proc.28.app4.1975

[22] Fagel, N., Boski, T., Likhoshway, L. and Oberhaensli, H. (2003) Late Quaternary Clay Mineral Record in Central Lake Baikal (Academician Ridge, Siberia). *Palaeogeography, Palaeoclimatology, Palaeoecology*, **193**, 159-179. https://doi.org/10.1016/s0031-0182(02)00633-8

[23] Arul Marcel Moshi, A., Ravindran, D., Sundara Bharathi, S.R., Indran, S. and Suganya Priyadharshini, G. (2020) Characterization of Surface-Modified Natural Cellulosic Fiber Extracted from the Root of Ficus Religiosa Tree. *International Journal of Biological Macromolecules*, **156**, 997-1006. https://doi.org/10.1016/j.ijbiomac.2020.04.117

[24] Klason, C., Kubát, J. and Strömvall, H. (1984) The Efficiency of Cellulosic Fillers in Common Thermoplastics. Part 1. Filling without Processing Aids or Coupling Agents. *International Journal of Polymeric Materials and Polymeric Biomaterials*, **10**, 159-187. https://doi.org/10.1080/00914038408080268

[25] Cheng, D., Weng, B., Chen, Y., Zhai, S., Wang, C., Xu, R., *et al.* (2020) Characterization of Potential Cellulose Fiber from Luffa Vine: A Study on Physicochemical and Structural Properties. *International Journal of Biological Macromolecules*, **164**, 2247-2257. https://doi.org/10.1016/j.ijbiomac.2020.08.098

[26] Jiang, Y., Deng, P., Jing, L. and Zhang, T. (2019) Tensile Properties and Structure Characterization of Palm Fibers by Alkali Treatment. *Fibers and Polymers*, **20**, 1029-1035. https://doi.org/10.1007/s12221-019-7841-3

[27] Saravanakumar, S.S., Kumaravel, A., Nagarajan, T., Sudhakar, P. and Baskaran, R. (2013) Characterization of a Novel Natural Cellulosic Fiber from *Prosopis juliflora* Bark. *Carbohydrate Polymers*, **92**, 1928-1933. https://doi.org/10.1016/j.carbpol.2012.11.064

[28] Pejic, B.M., Kostic, M.M., Skundric, P.D. and Praskalo, J.Z. (2008) The Effects of Hemicelluloses and Lignin Removal on Water Uptake Behavior of Hemp Fibers. *Bioresource Technology*, **99**, 7152-7159. https://doi.org/10.1016/j.biortech.2007.12.073

[29] Kuo, M.L., Mcclelland, J.F., Luo, S.Q., Chien, P.L., Walker, R.D. and Hse, C.Y. (1988) Applications of Infrared Photoacoustic-Spectroscopy for Wood Samples. *Wood and Fiber Science*, **20**, 132-145.

[30] Morán, J.I., Alvarez, V.A., Cyras, V.P. and Vázquez, A. (2007) Extraction of Cellulose and Preparation of Nanocellulose from Sisal Fibers. *Cellulose*, **15**, 149-159. https://doi.org/10.1007/s10570-007-9145-9

[31] Alvarez, V.A. and Vázquez, A. (2006) Influence of Fiber Chemical Modification Procedure on the Mechanical Properties and Water Absorption of Materbi-Y/Sisal Fiber Composites. *Composites Part A*: *Applied Science and Manufacturing*, **37**, 1672-1680. https://doi.org/10.1016/j.compositesa.2005.10.005

[32] Kostryukov, S.G., Matyakubov, H.B., Masterova, Y.Y., Kozlov, A.S., Pryanichnikova, M.K., Pynenkov, A.A., *et al.* (2023) Determination of Lignin, Cellulose, and Hemicellulose in Plant Materials by FTIR Spectroscopy. *Journal of Analytical Chemistry*, **78**, 718-727. https://doi.org/10.1134/s1061934823040093

[33] Fiore, V., Valenza, A. and Di Bella, G. (2011) Artichoke (*Cynara cardunculus* L.) Fibres as Potential Reinforcement of Composite Structures. *Composites Science and Technology*, **71**, 1138-1144. https://doi.org/10.1016/j.compscitech.2011.04.003

[34] Bukhari, A.A.H., Monier, M., Elsayed, N.H., Hashem, M.S., Eldiasty, J.G., Alnawmasi, J.S., *et al.* (2022) Flax Fiber Grafted with Cd(II)-Imprinted 2-Pyridylthiourea for Selective Ion Removal. *Materials Chemistry and Physics*, **287**, Article ID: 126239. https://doi.org/10.1016/j.matchemphys.2022.126239

[35] Rana, A.K., Basak, R.K., Mitra, B.C., Lawther, M. and Banerjee, A.N. (1997) Studies of Acetylation of Jute Using Simplified Procedure and Its Characterization. *Journal of Applied Polymer Science*, **64**, 1517-1523. https://doi.org/10.1002/(sici)1097-4628(19970523)64:8<1517::aid-app9>3.0.co;2-k

[36] Sawpan, M.A., Pickering, K.L. and Fernyhough, A. (2011) Effect of Various Chemical Treatments on the Fibre Structure and Tensile Properties of Industrial Hemp Fibres. *Composites Part A*: *Applied Science and Manufacturing*, **42**, 888-895. https://doi.org/10.1016/j.compositesa.2011.03.008

[37] Bouhank, S. (2017) Development of PVC/Spanish Broom Fiber Composite Materials: Formulations and Characterizations. Ph.D. Thesis, Process Engineering, Ferhat Abbas University—Setif 1, 130 p.

[38] Paiva, M., Ammar, I., Campos, A., Cheikh, R. and Cunha, A. (2007) Alfa Fibres: Mechanical, Morphological and Interfacial Characterization. *Composites Science and Technology*, **67**, 1132-1138. https://doi.org/10.1016/j.compscitech.2006.05.019

[39] Popescu, C., Larsson, P.T., Olaru, N. and Vasile, C. (2012) Spectroscopic Study of Acetylated Kraft Pulp Fibers. *Carbohydrate Polymers*, **88**, 530-536. https://doi.org/10.1016/j.carbpol.2011.12.046

[40] Rajeshkumar, G., Hariharan, V., Devnani, G.L., Prakash Maran, J., Sanjay, M.R., Siengchin, S., *et al.* (2021) Cellulose Fiber from Date Palm Petioles as Potential Reinforcement for Polymer Composites: Physicochemical and Structural Properties. *Polymer Composites*, **42**, 3943-3953. https://doi.org/10.1002/pc.26106

[41] Silva, M.C., Lopes, O.R., Colodette, J.L., Porto, A.O., Rieumont, J., Chaussy, D., *et al.* (2008) Characterization of Three Non-Product Materials from a Bleached Eucalyptus Kraft Pulp Mill, in View of Valorising Them as a Source of Cellulose Fibres. *Industrial Crops and Products*, **27**, 288-295. https://doi.org/10.1016/j.indcrop.2007.11.005

[42] Li, X., Tabil, L.G. and Panigrahi, S. (2007) Chemical Treatments of Natural Fiber for Use in Natural Fiber-Reinforced Composites: A Review. *Journal of Polymers and the Environment*, **15**, 25-33. https://doi.org/10.1007/s10924-006-0042-3

[43] Boumediri, H., Bezazi, A., Del Pino, G.G., Haddad, A., Scarpa, F. and Dufresne, A. (2019) Extraction and Characterization of Vascular Bundle and Fiber Strand from Date Palm Rachis as Potential Bio-Reinforcement in Composite. *Carbohydrate Polymers*, **222**, Article ID: 114997. https://doi.org/10.1016/j.carbpol.2019.114997

[44] Shahinur, S., Hasan, M., Ahsan, Q. and Haider, J. (2020) Effect of Chemical Treatment on Thermal Properties of Jute Fiber Used in Polymer Composites. *Journal of Composites Science*, **4**, Article 132. https://doi.org/10.3390/jcs4030132

[45] Ilangovan, M., Guna, V., Prajwal, B., Jiang, Q. and Reddy, N. (2020) Extraction and Characterisation of Natural Cellulose Fibers from Kigelia Africana. *Carbohydrate Polymers*, **236**, Article ID: 115996. https://doi.org/10.1016/j.carbpol.2020.115996

[46] Nenonene, A.Y. (2009) Development and Mechanical Characterization of Kenaf Stem Particleboard and Bioadhesives Based on Bone Glue, Tannin, or Mucilage. Ph.D. Thesis, University of Toulouse.

[47] Alawar, A., Hamed, A.M. and Al-Kaabi, K. (2009) Characterization of Treated Date Palm Tree Fiber as Composite Reinforcement. *Composites Part B*: *Engineering*, **40**, 601-606. https://doi.org/10.1016/j.compositesb.2009.04.018

[48] Budrugeac, P., Trandafir, V. and Albu, M.G. (2003) The Effect of the Hydration Degree on the Hydrothermal and Thermo-Oxidative Stability of Some Collageneous Matrices. *Journal of Thermal Analysis and Calorimetry*, **72**, 581-585. https://doi.org/10.1023/a:1024533801497

[49] Yang, H., Yan, R., Chen, H., Lee, D.H. and Zheng, C. (2007) Characteristics of Hemicellulose, Cellulose and Lignin Pyrolysis. *Fuel*, **86**, 1781-1788. https://doi.org/10.1016/j.fuel.2006.12.013

[50] Ramiah, M.V. (1970) Thermogravimetric and Differential Thermal Analysis of Cellulose, Hemicellulose, and Lignin. *Journal of Applied Polymer Science*, **14**, 1323-1337. https://doi.org/10.1002/app.1970.070140518

[51] Strezov, V., Moghtaderi, B. and Lucas, J.A. (2003) Thermal Study of Decomposition of Selected Biomass Samples. *Journal of Thermal Analysis and Calorimetry*, **72**, 1041-1048. https://doi.org/10.1023/a:1025003306775

[52] Ouajai, S. and Shanks, R.A. (2005) Composition, Structure and Thermal Degradation of Hemp Cellulose after Chemical Treatments. *Polymer Degradation and Stability*, **89**, 327-335. https://doi.org/10.1016/j.polymdegradstab.2005.01.016

[53] El may, Y., Jeguirim, M., Dorge, S., Trouvé, G. and Said, R. (2012) Study on the Thermal Behavior of Different Date Palm Residues: Characterization and Devolatilization Kinetics under Inert and Oxidative Atmospheres. *Energy*, **44**, 702-709. https://doi.org/10.1016/j.energy.2012.05.022

[54] Boutin, O., Ferrer, M. and Lédé, J. (1998) Radiant Flash Pyrolysis of Cellulose—Evidence for the Formation of Short Life Time Intermediate Liquid Species. *Journal of Analytical and Applied Pyrolysis*, **47**, 13-31. https://doi.org/10.1016/s0165-2370(98)00088-6

[55] Ray, D., Sarkar, B.K., Rana, A.K. and Bose, N.R. (2001) Effect of Alkali Treated Jute Fibres on Composite Properties. *Bulletin of Materials Science*, **24**, 129-135. https://doi.org/10.1007/bf02710089

[56] Das, M. and Chakraborty, D. (2007) Evaluation of Improvement of Physical and Mechanical Properties of Bamboo Fibers Due to Alkali Treatment. *Journal of Applied Polymer Science*, **107**, 522-527. https://doi.org/10.1002/app.26155

[57] Mwaikambo, L.Y. (2006) Review of the History, Properties and Application of Plant Fibers. *Science and Engineering Series*, **7**, 120-133.

[58] Saucier, C., Adebayo, M.A., Lima, E.C., Cataluña, R., Thue, P.S., Prola, L.D.T., *et al.* (2015) Microwave-Assisted Activated Carbon from Cocoa Shell as Adsorbent for Removal of Sodium Diclofenac and Nimesulide from Aqueous Effluents. *Journal of Hazardous Materials*, **289**, 18-27. https://doi.org/10.1016/j.jhazmat.2015.02.026